Available online at www.sciencedirect.com
ScienceDirect
Catalysis Today 125 (2007) 88–96
CATALYSIS TODAY
www.elsevier.com/locate/cattod

Study of the water-gas shift reaction on Mo_2C/Mo catalytic coatings for application in microstructured fuel processors

E.V. Rebrov [a,*], S.A. Kuznetsov [b], M.H.J.M. de Croon [a], J.C. Schouten [a]

[a] *Laboratory of Chemical Reactor Engineering, Eindhoven University of Technology, 5600 MB Eindhoven, The Netherlands*
[b] *Institute of Chemistry, Kola Science Centre RAS, 14 Fersman Str., 184209 Apatity, Murmansk Region, Russia*

Available online 17 April 2007

Abstract

The activity and stability of two types of molybdenum carbide coatings deposited on molybdenum substrates (Mo_2C/Mo) were compared in the water-gas shift reaction at 513–631 K. The activity of the Mo_2C/Mo coatings obtained by carburization of preoxidized molybdenum substrates in a CH_4/H_2 mixture at 973 K decreased to 20% of the initial value after 23 h on stream at 631 K in a mixture containing 0.5 vol.% CO, 1.5 vol.% H_2O and 40 vol.% H_2 balanced by helium. The activity of the Mo_2C/Mo coatings obtained by molten salt synthesis in a melt containing 5 wt.% Li_2CO_3 in an equimolar NaCl–KCl mixture at 1123 K for 7 h, was stable for more than 500 h on stream at similar reaction conditions. There was no evidence of methanation activity on both Mo_2C/Mo coatings below 621 K. The kinetics of the WGS and reverse WGS reactions was measured on Mo_2C/Mo coatings obtained by molten salt synthesis in a microstructured reactor operating in a differential mode. A combined power-law Eley–Rideal kinetic model is proposed to describe the reaction in the 531–631 K range. It was shown that, if molybdenum carbide is present as a thin layer over a molybdenum substrate (Mo_2C/Mo), the catalytic activity is enhanced compared to that of the pure Mo_2C phase.
© 2007 Elsevier B.V. All rights reserved.

Keywords: Water-gas shift; Molybdenum carbide; Molten salt synthesis; Microreactor; Kinetic study

1. Introduction

For portable and transport applications, the most convenient and economical way of hydrogen production is on-board reforming of hydrocarbon fuels in a fuel processor (FP) combined with a fuel cell (FC) stack, forming an integrated power supply device. In the reforming of gasoline or natural gas, a hydrogen-rich gas is produced with a carbon monoxide concentration of 8–12 vol.%. Because CO is a poison for a proton exchange membrane FC catalyst, the water-gas shift (WGS) reaction is used to reduce its concentration to below 1 vol.%, thereby increasing H_2 yield. A viable water-gas shift catalyst for an automotive fuel processor should demonstrate sufficient activity over a reasonable temperature window, have 5000 h stability, be non-pyrophoric (a feature not possessed by conventional Cu-based WGS catalysts), and not require a lengthy in situ pre-reduction procedure. Mo_2C catalysts showed higher activity for the WGS reaction than the commercial Cu/ZnO/Al_2O_3 catalyst [1–6], and high stability against oxidation under reaction conditions [7–9]. Recently, there have been a few reports about the promoting effect of cobalt and nickel [10,11]. However, their activity in the WGS decreases in the course of the reaction due to sintering of the promoted catalysts.

Investigation of molybdenum carbides was pioneered by Boudart's group [3,12,13]. They proposed that these carbides could be made through the direct carburization and temperature programmed reduction (TPR) of bulk MoO_3 by flowing a gas mixture of 20 vol.% CH_4 in H_2 over the sample at 973 K [3]. This process yields Mo_2C nanoparticles of ca. 12 nm [12]. Similar TPR methods with a mixture of 20 vol.% CH_4 (balance H_2) have been used to form alumina supported Mo_2C [13]. This involved first impregnating γ-Al_2O_3 with ammonium heptamolybdate, followed by calcination in air at 773 K for 5 h. The catalyst is then carburized using TPR in a 20 vol.% CH_4 in hydrogen mixture up to 1173 K. However, the activity of the Mo_2C catalysts per unit rector volume is limited by its low surface area [3]. Therefore, a synthesis method should be developed that yields high-surface-area carbides. In principle, molybdenum carbides with high BET surface area can be obtained via a high temperature sintering by hot isostatic pressing (HIP), chemical

* Corresponding author. Tel.: +31 40 2472850.
E-mail address: e.rebrov@tue.nl (E.V. Rebrov).

0920-5861/$ – see front matter © 2007 Elsevier B.V. All rights reserved.
doi:10.1016/j.cattod.2007.01.075

vapour deposition (CVD), microwave assisted synthesis [14], molten salt synthesis [15,16], and some other methods [17–20]. Electrochemical synthesis from molten salts offers considerable advantages over other methods [15]. For example, electrochemical methods such as pulse plating and reversed plating provide a possibility to control the structure and phase composition, the thickness of the coatings, the grain size (down to nanoscale), porosity, smoothness, and the texture of the layer. The other advantages are: (i) relatively low synthesis temperature (973–1023 K); (ii) parameters of electrochemical depositions can be easily adapted in scaling-up synthesis; (iii) the method can be applied to substrates with a complicated geometry (such as microstructured plates) for obtaining of uniform coatings with respect to thickness, grain size and composition of the layer; (iv) high purity of resulting coatings even with low-grade initial reactants. It is also of importance that the production costs are much lower, as compared to other methods.

The integration of reaction and heat exchange within one piece of equipment has basic advantages over the conventional unit operation design. Tonkovich et al. [21] investigated the possibility of the application of a microreactor for the WGS reactor in fuel processing applications. The authors concluded that a WGS microstructured reactor for a fuel processor can approach sizes one-to-two orders of magnitude smaller than conventional fixed bed reactors. However, much more active catalytic coatings as compared to conventional systems, have to be developed in order to reach a two orders of magnitude size reduction of a WGS reactor. Delsman et al. proposed the design of a preferential oxidation microdevice for the preferential oxidation of CO in a hydrogen-rich gas for a portable fuel processor [22]. The microdevice consists of an isothermal microreactor and two counter current heat exchangers, which enables a high heat recovery efficiency of 90%.

This paper focuses on the study of activity and stability of two series of Mo_2C catalytic coatings prepared on Mo substrate by different methods. The first series was made by in situ reduction of a MoO_3 coating by a CH_4/H_2 mixture at 973 K [3]. In turn, MoO_3 coatings were obtained by oxidation of the Mo substrates with an air–water mixture [23]. The second series was made by direct reduction of Mo substrates in an ionic melt containing a carbon source. Based on the water-gas shift (WGS) and reverse water-gas shift (RWGS) kinetics on a Mo_2C/Mo catalyst, a combined power-law Eley–Rideal (PL ER) kinetic model was derived in the temperature range of 531–631 K. This kinetic model was integrated in a reactor model for design of a full-scale WGS microstructured reactor/heat-exchanger. Modeling results indicated that application of a microreactor with the Mo_2C/Mo catalyst in the temperature range above 523 K can convert up to 75% of CO present in the flow stream decreasing the size of the downstream low temperature (LT) WGS unit.

2. Experimental

2.1. Synthesis of Mo_2C/Mo coatings

Molybdenum sheets (99.99+ wt.% Mo) of 40 mm length, 9 mm width, with a thickness of 100 μm were used as substrates. Molybdenum samples were cleaned in xylene for 1 h to remove organic contaminations from the surface, dried in an oven at 413 K, and weighed.

2.1.1. Series A: carburization of MoO_3

The cleaned plates were oxidized in a dry air flow of 50 ml/min at 673 K for 16 h. Above 623 K in the presence of oxygen, molybdenum oxidizes to the thermodynamically most stable oxide, orthorhombic MoO_3 [24]. An XRD pattern (see Fig. 1a) confirmed formation of a MoO_3 coating. The SEM data (not shown) revealed that the thickness of the MoO_3 layer was 10 μm. The oxidized plates were inserted in a microreactor, pretreated in a He flow of 50 ml/min at 773 K for 1 h, then the reactor was cooled down to 300 K. The He flow was replaced by a mixture of 20 vol.% CH_4 in hydrogen flowing at 50 ml/min. Subsequently, the reactor temperature was increased from 300 to 973 K with a heating rate of 1 K/min, and the reactor was kept at 973 K for 30 min. At the end of the reduction period, the CH_4/H_2 flow was replaced by hydrogen, and the temperature was decreased to the reaction temperature. Finally, the hydrogen flow was replaced by the reaction mixture. The XRD pattern (see Fig. 1b) confirmed formation of the hexagonal Mo_2C phase. Fig. 1b shows the XRD patterns of the as-prepared Mo_2C. The eight strong peaks at 2θ of 34.37°, 37.93°, 39.41°, 52.11°, 61.57°, 69.51°, 74.64°, and 75.60° can be indexed as hexagonal Mo_2C (0 1 0), (0 0 2), (0 1 1), (0 1 2), (1 1 0), (0 1 3), (1 1 2), and (0 2 1), with lattice constants $a = 3.008$ Å and $c = 4.131$ Å, in good agreement with $a = 3.006$ Å and $c = 4.733$ Å (JCPDS card no. 11–0680). In addition, there are obviously two peaks in Fig. 1b at 2θ of 37.11° and 43.12°. These diffraction lines can be indexed as a cubic phase of Mo_2C (1 1 1), (0 0 2). The lattice constant was $a = 4.19$ Å, close to $a = 4.155$ Å (JCPDS card no. 15-0457). Therefore, the product was mainly hexagonal or β-Mo_2C with a small amount (below 10 wt.%) of cubic Mo_2C. The thickness of the resulting carbide layer, according to the SEM data, is ca. 4 μm. The BET surface area of the Mo_2C layer is 19 $m^2\ g^{-1}$.

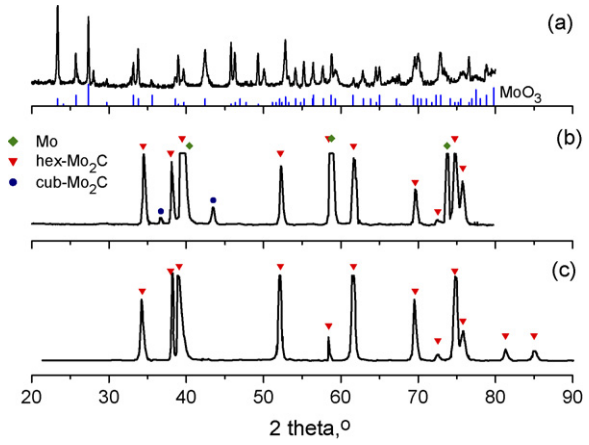

Fig. 1. XRD patterns of the substrates: (a) after oxidation in a dry air flow of 50 ml min^{-1} at 673 K for 16 h; (b) after reduction of oxidized samples in a mixture of 20 vol.% CH_4 in hydrogen at 973 K for 30 min; (c) after molten salts synthesis in a Li_2CO_3 (5 wt.%) NaCl–KCl equimolar mixture at 1123 K for 7 h with a cathodic current density of 5 mA cm^{-2}.

The catalyst volume per plate is 2.9–10^{-3} cm^3 corresponding to the apparent density of the Mo_2C layer of 2.5 g cm^{-3}.

2.1.2. Series B: molten salt synthesis

Carburization of molybdenum substrates was carried out in a melt consisting of a NaCl–KCl equimolar mixture, and Li_2CO_3 (5 wt.%). Sodium and potassium chlorides were mixed in the required ratio, placed in a glassy carbon ampoule (SU-2000 type) and transferred to a sealed stainless steel retort. The latter was evacuated to a residual pressure of 0.67 Pa at 873 K. The molybdenum substrates were immersed in the NaCl–KCl equimolar melt through a special opening in the top part of the retort under inert atmosphere. Synthesis of Mo_2C on molybdenum substrates was performed at 1123 K, for 7 h with a cathodic current density of 5 mA cm^{-2}. The details on the synthesis are reported elsewhere [25]. Hexagonal Mo_2C was the only phase present in the coatings (see Fig. 1c, JCPDS card no. 11-0680). The morphology of the Mo_2C layer is shown in Fig. 2. The BET surface area is 18 m^2 g^{-1}. The catalyst volume per plate is 4.0×10^{-4} cm^3 corresponding to the apparent density of the Mo_2C layer of 4.0 g cm^{-3}.

2.2. Catalytic activity measurements

The reactor has an AISI 316 stainless steel housing with standard tube connections and can be heated up to 923 K with an electrical furnace. Twenty cavities of 130 μm × 400 μm were microfabricated by electrical discharge machining (EDM) in the side walls of the reactor compartment along the length of the reactor (Fig. 3). The activity tests were carried out at atmospheric pressure either with four, eight, or sixteen Mo_2C/Mo plates inserted in the microstructured reactor. To attain the desired amounts of water vapour in the gas feed mixture, a helium flow was fed through a saturator, which was kept at a desired temperature. The overall flow rate was set at 50 ml/min. The total volume of catalyst A was 4×10^{-2} cm^3 corresponding to a GHSV of 75,000 h^{-1}. The total volume of catalyst B was either 1.6, 3.2, or 6.4×10^{-3} cm^3 corresponding to space velocities between 470,000 and 1,800,000 h^{-1}. WHSV (weight of feed per hour per weight of catalyst) depends on the feed molar composition. It can be estimated based on an average fluid density of 0.12 g/m^3 (STP) and an apparent catalyst density of 4.0 g/m^3. Therefore, WHSV = 0.03 GHSV. The temperature was measured by a thermocouple located at the centerline of the reactor. The kinetic parameters of the forward and reverse WGS reactions were measured at conversions below 15%. The concentrations of the components in the effluent gas were analyzed with a Varian GC (CP-3800), equipped with TCD detectors. Helium was used as a carrier gas and nitrogen was used as an internal standard. N_2, CH_4, H_2, and CO were analyzed on a molsieve 5A column (0.25 mm i.d., 10 m). CO_2 and H_2O were analyzed on a poraPLOT-U column (0.25 mm i.d., 10 m). The column temperature was initially held at 343 K for 3 min, after which it was increased from 343 to 453 K at a rate of 40 K/min, then held at 453 K for 5 min. The carbon mass balances were closed within 95%. The reaction rates were calculated from the product analysis using the differential reactor approximation.

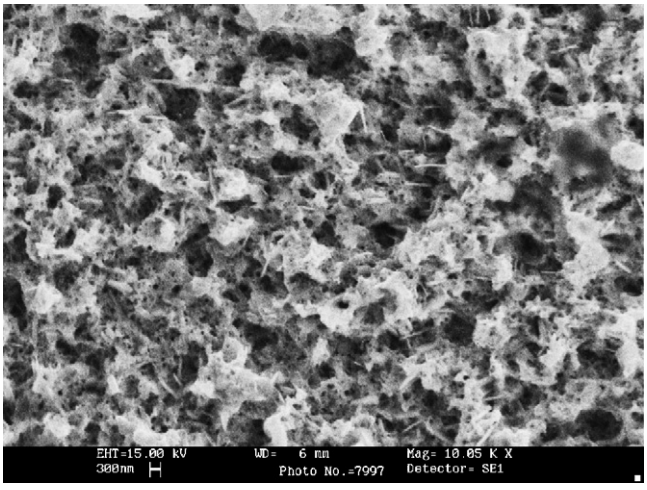

Fig. 2. SEM image of Mo_2C/Mo coating obtained by molten salts synthesis in a Li_2CO_3 (5 wt.%) NaCl–KCl equimolar mixture at 1123 K for 7 h with a cathodic current density of 5 mA cm^{-2}.

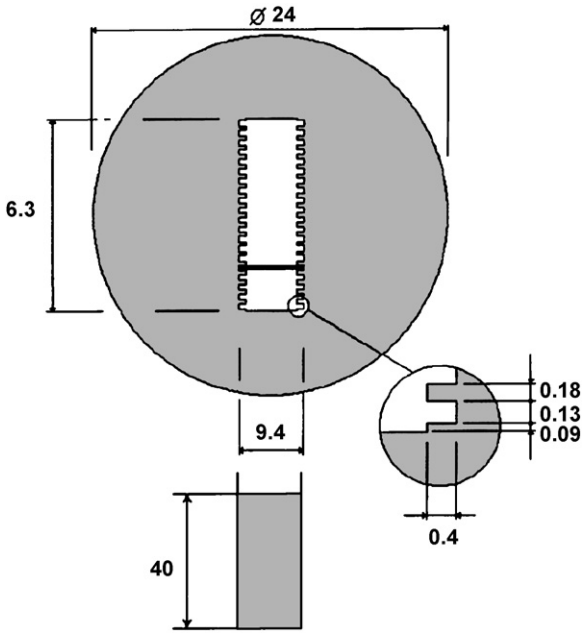

Fig. 3. Front view of the AISI 316 plate-type microreactor with a single molybdenum plate. The frame represents the part of the microreactor at high magnification. All dimensions are in millimeters and are not on scale.

2.3. Characterization

Different phases were identified by X-ray diffraction analysis on a Rigaku Geigerflex diffractometer using Cu Kα radiation (k = 1.5405 Å, voltage 40 kV, and current 30 mA) with continuous scanning at a rate of 2° 2θ/min in the range of 20–80° 2θ. The morphology as well as the layer thickness of the Mo_2C coatings were examined by SEM on a JEOL JSM-840A microscope. The adsorption isotherms were obtained on an ASAP-2000 Micromeritics instrument with a standard procedure after vacuum pretreatment at 573 K for 12 h up to a residual pressure less than 0.1 Pa. The surface area of the

coating was measured by the BET method at 77 K, with N_2 as the adsorbent.

3. Results and discussion

3.1. Catalytic activity of the coatings in the WGS reaction

On series A, the activity in the WGS reaction decreased to 20% of the initial value after 23 h operation at 631 K in a mixture containing 0.5 vol.% CO, 1.5 vol.% H_2O and 40 vol.% H_2, balanced by helium (Fig. 4). Catalyst treatment in a hydrogen flow at 773 K for 1 h completely restored the initial activity, however the activity decreased again to the same level after 23 h on stream at 631 K. Moon and Ryu [2] reported that the deactivation of the supported Mo_2C catalyst is caused by the transition of $Mo^{\delta+}$ ($IV < \delta^+ < VI$) from Mo^{IV} (MoO_xC_y), and Mo_2C to Mo^{VI} (MoO_3) by the reaction with H_2O. Thus, it appears that the carbide layer is monotonously oxidized by the reaction mixture at these conditions. The activity of catalysts series B was stable for more than 500 h on stream at similar reaction conditions. Fig. 5 compares the WGS reaction rate over Mo_2C/Mo coatings of both series after 23 h on stream with those over the bulk Mo_2C catalyst and commercial Cu/ZnO/Al_2O_3 catalyst [1]. It can be seen that steady-state specific reaction rates for the Mo_2C/Mo coatings are higher than those observed on the commercial Cu/ZnO/Al_2O_3 catalyst and Mo_2C bulk catalyst. Apparent activation energies for both Mo_2C coatings of 63 ± 2 kJ/mol (series A and B) were close to those reported for both the bulk Mo_2C and Cu/ZnO/AI_2O_3 (71 ± 8 kJ/mol) [1]. No methanation reaction takes place on coating series B up to 631 K. On the coating series A, the onset of methanation occurs at 612 K. The turnover rates of coating series A were still three times higher than those reported for the bulk Mo_2C catalysts [1]. These results demonstrate that if molybdenum carbides are present as a thin layer over a molybdenum substrate, the specific catalytic activity can be enhanced by an order of magnitude comparing to that of the pure Mo_2C phase. Furthermore, the coatings prepared in different ways behave in a distinctly different manner.

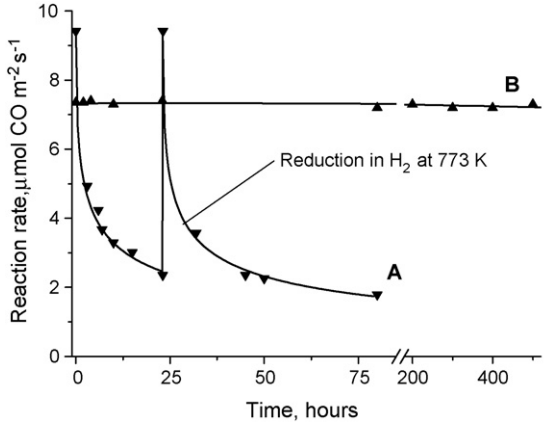

Fig. 4. Time-on-stream testing of catalysts for the WGS reaction at 631 K in a mixture containing 0.5 vol.% CO, 1.5 vol.% H_2O and 40 vol.% H_2, balanced by helium. Total flow: 50 cm^3 min^{-1} (STP).

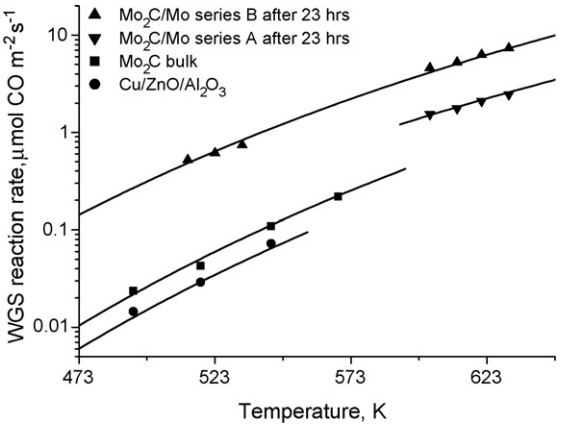

Fig. 5. Comparison of the WGS reaction rate on the Mo_2C/Mo coatings series A and B after 23 h on-stream with those on the bulk Mo_2C and commercial Cu/ZnO/Al_2O_3 catalyst taken from [1]. The CO conversion ranged from 2 to 15% on the Mo_2C/Mo coatings. Reaction conditions: $p_{CO} = 0.2$ kPa, $p_{H_2O} = 0.7$ kPa, $p_{H_2} = 40$ kPa, balance—He. Total flow: 50 cm^3 min^{-1} (STP). The CO conversion ranged between 2 and 30% on the bulk Mo_2C and Cu/ZnO/Al_2O_3 catalysts. Reaction conditions: $p_{CO} = 5.7$ kPa, $p_{H_2O} = 31.8$ kPa, $p_{H_2} = 62.5$ kPa. Total flow: 56 cm^3 min^{-1} (STP).

However, the optimization of the preparation method was beyond the scope of the present study. An attempt was made to improve the performance of the WGS reactor by utilizing the favourable catalytic properties of the Mo_2C coatings above 523 K, where the Cu/ZnO/Al_2O_3 catalyst cannot be used due to the sintering of the dispersed copper particles. The kinetics of the WGS and RWGS reactions was studied separately in two different set of conditions. For the WGS reaction, the equilibrium parameter β (Eq. (1)) was always below 0.05, so the kinetics was not expected to be affected by a reversible reaction:

$$\beta = \frac{p_{CO_2} p_{H_2}}{K_p p_{CO} p_{H_2O}} \quad (1)$$

When operating far from equilibrium, even despite the non-linearity of a complex reaction system, the overall rate of a heterogeneous catalytic reaction can be expressed by a classical equation, where the equilibrium constant is determined by the ratio of constants of the forward and reverse reactions [26].

3.2. Kinetic study of the WGS reaction

The kinetic study has been carried out on catalyst B. A reaction order of one (0.97 ± 0.03) with respect to CO was found in a temperature range of 612–631 K, which does not depend on the temperature and H_2O/CO ratio for CO partial pressures between 250 and 450 Pa, corresponding to H_2O/CO ratios between 1.5 and 3. As the temperature decreases, the CO reaction order slightly decreases to 0.79 ± 0.03. In the temperature range between 513 and 533 K, the reaction order with respect to CO was studied by varying the CO partial pressure between 200 and 400 Pa at three different p_{H_2O} of 430, 580 and 700 Pa to provide H_2O/CO ratios between 1.5 and 3 (Fig. 5). Thus far, CO_2 was not included in the feed, which will certainly be a component of interest in a real feed stream. The

H_2O/CO ratios are lower than those used in the commercial LT WGS processing of the gas exiting HT WGS. We have done this for two reasons. The first is that we did not use CO_2 in the feed. Hence, we could lower the H_2O/CO ratio because there was no need to compensate the CO_2 influence on equilibrium with higher H_2O concentration. Secondly, we wanted to study the behavior of WGS coatings at close to stoichiometric H_2O/CO ratio in order to investigate the influence of H_2O partial pressure on the WGS kinetics. In general, the feed composition used in this study was similar to that reported in [27,28], except that the CO concentration and the H_2O/CO ratio were lower. It was found that the reaction becomes 0.79 ± 0.03 order in CO at H_2O/CO ratios above 1.5, whereas at H_2O/CO ratios close to 1, the reaction order with respect to CO slightly decreases from this value.

The partial pressure of H_2O was varied from 430 till 700 Pa at 513 and 523 K (Fig. 7). At H_2O/CO ratios above 1.5, the reaction order in H_2O remains nearly the same. It is equal to 0.5 for the two different partial pressures of CO. A power-law (PL) rate model for the WGS reaction at H_2O/CO ratios above 1.5 can be written as

$$r_{\mathrm{WGS}} = k_{\mathrm{F}}^{0}\, \mathrm{e}^{-E_{\mathrm{F}}/RT}\, p_{\mathrm{CO}}^{0.9}\, p_{\mathrm{H_2O}}^{0.5} \tag{2}$$

where k_{F}^{0} is the pre-exponential factor, and E_{F} is the apparent activation energy of the WGS reaction, respectively. The comparison between the experimental and predicted reaction rates are shown in Figs. 6 and 7. A good agreement is observed between the measurements and predictions of the PL model. The parameters values are listed in Table 1. It should be noted that the reaction orders are close to those reported by Keiske et al. for a Fe_3O_4–Cr_2O_3 catalyst [29].

3.3. Kinetic study of the RWGS reaction

The reaction order in H_2 increases from 0.3 to 2 with increasing hydrogen partial pressure from 22 to 44 kPa (Fig. 8). To explain this dependence of reaction order, a red–ox

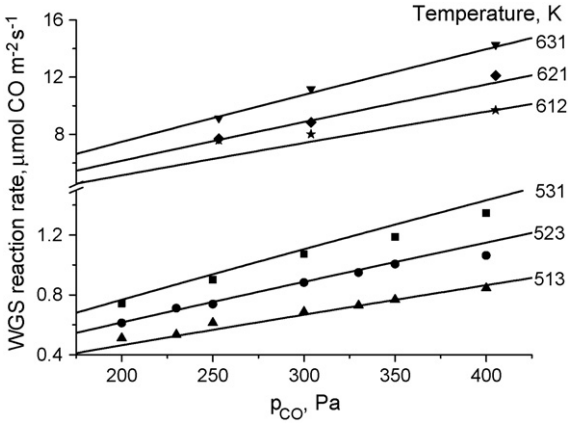

Fig. 6. WGS reaction rate on the Mo_2C/Mo coatings series B as a function of the CO partial pressure at various temperatures. Reaction conditions: $p_{\mathrm{CO}} = 0.20 - 0.40$ kPa, $p_{\mathrm{H_2O}} = 0.70$ kPa, $p_{\mathrm{H_2}} = 40.0$ kPa, balance—He. Total flow: 50 $\mathrm{cm^3\ min^{-1}}$ (STP). Symbols represent the experimental data whereas solid lines represent the fits according to the model given by Eq. (2).

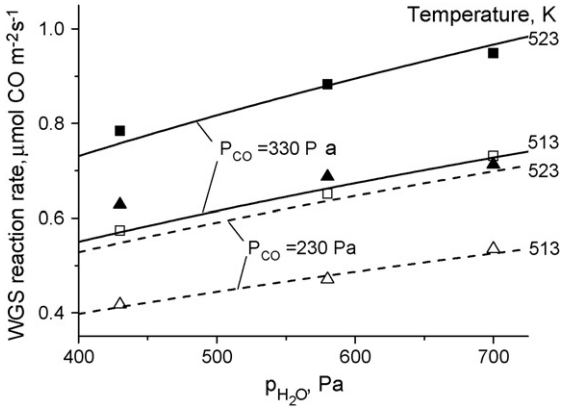

Fig. 7. WGS reaction rate on the Mo_2C/Mo coatings series B as a function of the water partial pressure at 513 and 523 K. Open symbols represent the experimental data at p_{co} of 0.23 kPa; closed symbols represent the experimental data at p_{co} of 0.33 kPa. The other reaction conditions are the same as those in Fig. 5. The dashed lines represent the fits according to the model given by Eq. (2) at p_{co} of 0.23 kPa. The solid lines represent those at p_{CO} of 0.33 kPa.

mechanism is proposed. According to this mechanism, the catalyst is reversibly reduced under increasing hydrogen pressure and oxidizes when the hydrogen pressure decreases below some critical value, which depends on the water content in the feed Eq. (3):

$$[\mathrm{M}] + \mathrm{H_2O} \xrightarrow{K_{\mathrm{M}}} [\mathrm{M-O}] + \mathrm{H_2} \tag{3}$$

where [M] represents a surface metal site and [M − O] represents an oxidized metal site. Under steady state conditions, the relative amount of the oxidized (ϑ_{OX}) and reduced (ϑ_{RED}) sites depends on the equilibrium constant K_{M}, and the H_2/H_2O ratio Eq. (4):

$$\vartheta_{\mathrm{OX}} = \frac{1}{1 + K_{\mathrm{M}}(p_{\mathrm{H_2}}/p_{\mathrm{H_2O}})}, \qquad \vartheta_{\mathrm{RED}} = \frac{K_{\mathrm{M}}(p_{\mathrm{H_2}}/p_{\mathrm{H_2O}})}{1 + K_{\mathrm{M}}(p_{\mathrm{H_2}}/p_{\mathrm{H_2O}})} \tag{4}$$

The RWGS reactions takes place on both sites Eq. (5):

$$r_{\mathrm{RWGS}} = \vartheta_{\mathrm{OX}} r_{\mathrm{RWGS\text{-}OX}} + \vartheta_{\mathrm{RED}} r_{\mathrm{RWGS\text{-}RED}} \tag{5}$$

A sharp increase in RWGS reaction rate, observed at hydrogen partial pressures above 30 kPa, is a strong evidence in favour of the red-ox mechanism. In the range of H_2/H_2O pressures studied, the contribution from the reduced sites dominates, $\vartheta_{\mathrm{OX}} r_{\mathrm{RWGS\text{-}OX}} \ll \vartheta_{\mathrm{RED}} r_{\mathrm{RWGS\text{-}RED}}$, so the first term in Eq. (5) can be omitted. The rate of the RWGS reaction on the reduced sites can be described by an Eley–Rideal (ER) model

Table 1
Kinetic parameters for the lumped reaction model

Parameter	Value
k_{F}^{0} ($\times 10^2$ μmol $\mathrm{Pa^{-1.4}\ m^{-2}\ s^{-1}}$)	4.18
E_{F} (kJ $\mathrm{mol^{-1}}$)	63.4 ± 2.0
$k_{\mathrm{B}}^{0\prime}$ ($\times 10^5$ μmol $\mathrm{Pa^{-1}\ m^{-2}\ s^{-1}}$)	3.16
E_{B} (kJ $\mathrm{mol^{-1}}$)	114.0 ± 3.5
$K_{\mathrm{CO_2}}$ ($\mathrm{Pa^{-1}}$)	$-0.0164 + 6.544 \times 10^{-5} T - 6.154 \times 10^{-8} T^2$

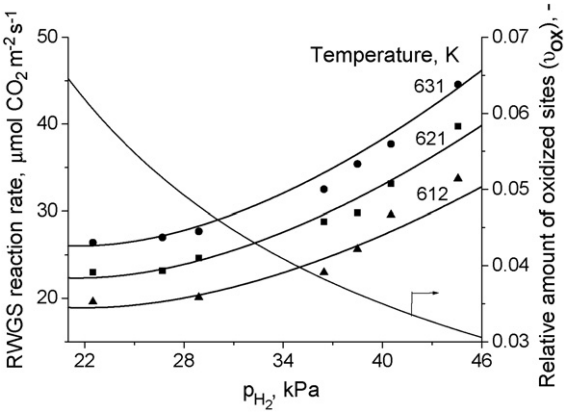

Fig. 8. RWGS reaction rate on the Mo_2C/Mo coatings series B as a function of the hydrogen partial pressure. Reaction conditions: $p_{CO_2} = 1.30$ kPa, $p_{H_2O} = 1.45$ kPa, $p_{H_2} = 22.045.0$ kPa, balance—He. Total flow: 50 cm^3 min^{-1} (STP). Symbols represent the experimental data whereas solid lines represent the fits according to the model given by Eq. (5).

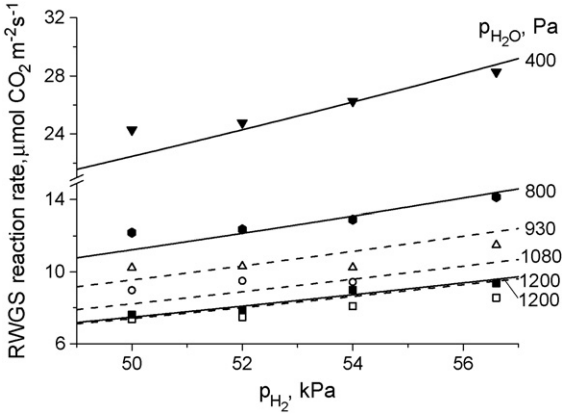

Fig. 10. RWGS reaction rate on the Mo_2C/Mo coatings series B as a function of the hydrogen partial pressure. Reaction conditions: $p_{CO_2} = 0.10$ kPa, $p_{H_2} = 50.0 - 56.6$ kPa, $p_{H_2O} = 0.401.20$ kPa, balance—He. Total flow: 50 cm^3 min^{-1} (STP). Open and closed symbols represent the experimental data at 626 and 631 K, respectively. Dashed and solid lines represent the fits according to the model given by Eq. (7) at 626 and 631 K, respectively.

with adsorbed CO_2 on the surface sites, which reacts with hydrogen from the gas phase (Eq. (6), see Fig. 9):

$$r_{\text{RWGS-RED}} = \frac{k_{\text{R-RED}} K_{CO_2} p_{CO_2} p_{H_2}}{1 + K_{CO_2} p_{CO_2}} \quad (6)$$

In the range of hydrogen partial pressures above 35 kPa, the RWGS reaction is second order in hydrogen partial pressure (see Fig. 9). Therefore, the equation for the RWGS can be rewritten as

$$r_{\text{RWGS}} = \frac{k K_{\text{M}} K_{CO_2} p_{CO_2} p_{H_2}^2}{(1 + K_{CO_2} p_{CO_2}) p_{H_2O}} \quad (7)$$

The rate of the RWGS reaction was found to decrease on the addition of water to the reaction mixture of CO_2 and H_2 (Fig. 10). In this study, effect of water on the rate of the RWGS was investigated at H_2O/CO_2 ratios of 4–14 at 621 and 626 K. It can be seen that addition of water considerably reduces the RWGS reaction.

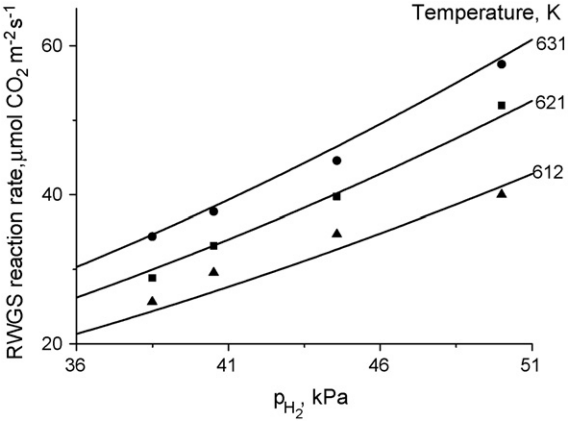

Fig. 9. RWGS reaction rate on the Mo_2C/Mo coatings series B as a function of the hydrogen partial pressure. Reaction conditions: $p_{H_2} = 38.550.0$ kPa, other conditions are the same as those in Fig. 8. Symbols represent the experimental data whereas solid lines represent the fits according to the model given by Eq. (7).

The CO_2 reaction order of was determined in the RWGS reaction by varying the CO_2 partial pressure between 1.5 and 2.5 kPa at a constant hydrogen pressure of 22.2 kPa (see Fig. 11). The reaction order with respect to CO_2 monotonously increases from 0.35 at 533 K to 0.64 at 631 K. The temperature dependence of the adsorption constant K_{CO_2} was fitted by a second order polynomial function (see Table 1) in order to describe the change in CO_2 reaction order with temperature. Combining now Eqs. (2) and (7), the overall rate of the reaction (r_{ov}) can be expressed as

$$r_{\text{OV}} = k_{\text{F}}^0 \, e^{-E_{\text{F}}/RT} \, p_{CO}^{0.9} \, p_{H_2O}^{0.5} - \frac{k_{\text{R}}^{0'} \, e^{-E_{\text{R}}/RT} \, p_{CO_2} \, p_{H_2}^2}{(1 + K_{CO_2} p_{CO_2}) p_{H_2O}} \quad (8)$$

One of the critical aspects in optimization of the WGS using a kinetic model is to accurately capture the reaction equilibrium. Since the reaction rate equation of the WGS

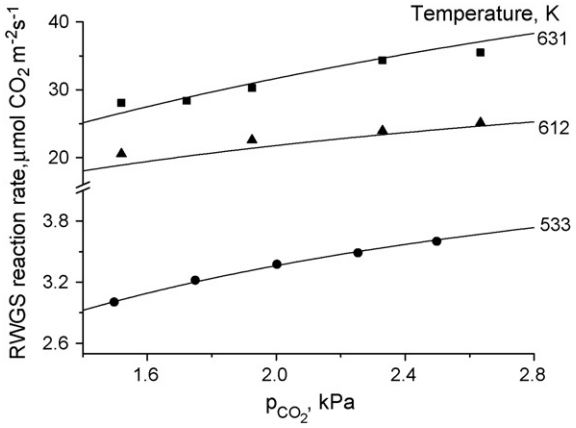

Fig. 11. RWGS reaction rate on the Mo_2C/Mo coatings series B as a function of the CO_2 partial pressure. Reaction conditions: $p_{CO_2} = 1.52.5$ kPa, $p_{H_2} = 22.2$ kPa, balance—He. Total flow: 50 cm^3 min^{-1} (STP). p_{H_2O} at 533 K was 0.20 kPa, p_{H_2O} at 612–631 K was 0.70 kPa. Symbols represent the experimental data. Solid lines represent the fits according to the model given by Eq. (7).

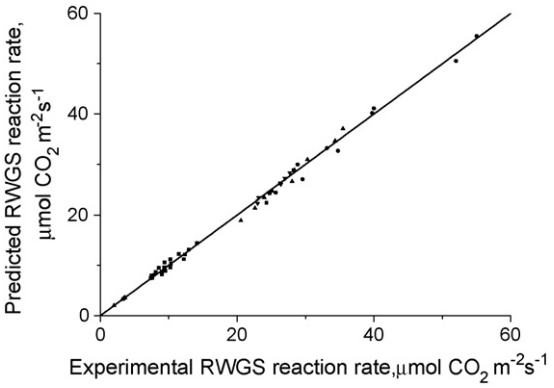

Fig. 12. Predicted vs. experimental values of RWGS reaction rate on the Mo_2C/Mo coatings series B. The reaction conditions are taken from Figs. 8–11.

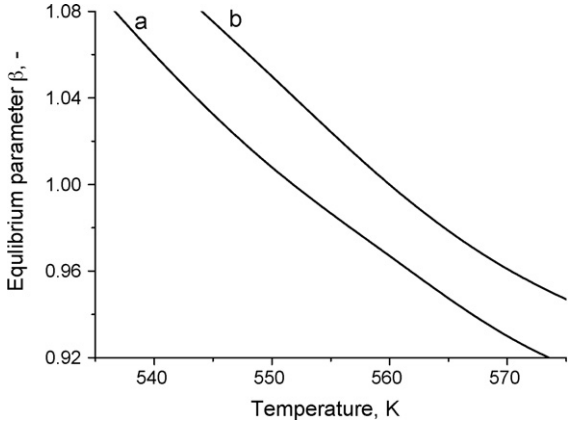

Fig. 13. The equilibrium parameter (β, see Eq. (1)) as a function of reaction temperature. Reaction conditions: (a) $p_{CO} = 1.0$ kPa, $p_{H_2O} = 2.0$ kPa, $p_{CO_2} = 1.0$ kPa, $p_{H_2} = 57$ kPa, balance—He; (b) $p_{CO} = 1.0$ kPa, $p_{H_2O} = 2.5$ kPa, $p_{CO_2} = 1.0$ kPa, $p_{H_2} = 62$ kPa, balance—He.

and RWGS are formulated, the thermodynamic consistency can be checked for the overall WGS reaction. Although the number of data sets were limited, the parity plot for the RWGS reaction (Fig. 12) shows that the model describes the measured data reasonably well. The parameter values for the RWGS reaction are listed in Table 1. Generally, the higher the hydrogen content in the feed, the higher H_2O/CO ratio is required. Fig. 13 shows the plots for the thermodynamic consistency for the overall reaction for H_2O/CO of 2 and 2.5 at hydrogen partial pressures of 57 and 62 kPa, respectively. Eq. (9) predicts the equilibrium CO conversion rather good in the temperature range between 540 and 580 K. With decreasing H_2O/CO ratio below 1.5, the range of the thermodynamic consistency also decreases, which is related to the power law character of the kinetic equation of the forward WGS reaction. Actually, the assumption of constant reaction order in water is no longer valid, resulting in a poor description of the equilibrium CO conversion at H_2O/CO ratios below 1.5.

3.4. Comparison of Mo_2C/Mo with Cu/ZnO/Al_2O_3

It is interesting to compare the activity of Mo_2C/Mo and the commercial Cu–ZnO–Al_2O_3 catalyst per unit of reactor volume. It should be noted that operation of the Cu–ZnO–Al_2O_3 catalyst is limited to 523 K while the Mo_2C/Mo catalyst can be used in the temperature range up to 631 K. To demonstrate the performance of the two systems, a comparison is made between an adiabatic fixed bed reactor with the Cu–ZnO–Al_2O_3 catalyst and an isothermal microstructured reactor, operating at the top limit of the temperature range used in commercial technology, viz. 523 K (see Table 2). An average bed temperature for the fixed bed reactor was estimated to be 500 K for the fresh Cu/ZnO/Al_2O_3 catalyst, assuming that it can be increased to 523 K as the catalyst deactivates. The heat capacity of the fluid was calculated for a mixture of 2 vol.% CO, 13 vol.% CO_2, 33 vol.% H_2O, 52 vol.% H_2. A PL reaction rate equation for a Cu/ZnO/Al_2O3 catalyst was taken from [30]. The CO conversion in both cases was 50%.

It can be seen, that the catalysts show a similar CO removal rate per unit of reactor volume. However, there is still enough room to improve the performance of the Mo_2C/Mo coatings. First of all, the distance between the flow passages (see Fig. 3) can be considerably reduced if the microchannels would be machined directly in the molybdenum plates. This can increase the catalyst loading in the reactor by a factor of 3. Second, the coating thickness can be increased up to 5–10 μm without considerable decrease in the catalyst surface area. To reach this goal, the parameters of molten salt synthesis have to be adjusted. There is also the possibility to introduce a second

Table 2
Comparison of Mo_2C/Mo and Cu/ZnO/Al_2O_3 catalysts

Parameter	Mo_2C/Mo	Cu/ZnO/Al_2O_3
Temperature range (K)	523–650	433–523
Apparent density (kg m^{-3})	4.0×10^3	1.1×10^3
BET surface area (m^2 g^{-1})	18	60
Part of the reactor occupied by the catalyst (%)	1.2[a]	100
Catalyst specific surface area in the reactor (m^2 m^{-3})	8.7×10^5	6.6×10^7
Overall WGS reaction rate (μmol m^{-2} s^{-1})	0.015[b]	0.8[c]
CO removal rate (mol m^{-3} s^{-1})	0.7	1.0

[a] Based on the geometry shown in Fig. 3.
[b] Isothermal operation at 523 K
[c] Average reactor rate in an adiabatic fixed bed reactor. An average bed temperature for the fixed bed reactor was estimated to be 500 K for the fresh Cu/ZnO/Al_2O_3 catalyst, assuming that it can be increased to 523 K as the catalyst deactivates. The Cp was calculated for a mixture of 2 vol.% CO, 13 vol.% CO_2, 33 vol.% H_2O, 52 vol.% H_2. A PL reaction rate equation for a Cu/ZnO/Al_2O_3 catalyst was taken from [30].

metal which can preserve the surface area of the coatings [10,11]. If successful, this can lead to a two- to three-fold increase of the catalyst loading in the microreactor, compared to the present concept. Finally, there is a possibility to create a desired temperature gradient in the microstructured reactor. While the two-stage design of a WGS system is standard practice, recently, much work has focused on optimization of this system, especially in the context of determining an optimum temperature profile [31–33]. The CO conversion is equilibrium-limited at high temperatures and kinetically limited at low temperatures. That means that isothermal operation initially yields conversions lower than those obtained adiabatically, but the conversion curve for the isothermal case continues to increase well beyond the point at which the conversion profile for the adiabatic case reaches a plateau. The WGS reaction is an exothermic equilibrium reaction and the equilibrium conversion decreases with increasing temperature. Therefore, a significantly better performance can be achieved by operating at a relatively high temperature, thereby exploiting reaction kinetics when the gas composition is far from equilibrium, and then lowering the temperature as thermodynamics begins to limit the CO conversion. Therefore, the reactor temperature should be decreased along the reactor coordinate in agreement with the reaction kinetics to decrease the reactor volume (Fig. 13). This can be done by combining the reactor with a counter-current heat-exchanger in a single unit [31,32] as well as by optimization of the process layout and operating conditions with internal heat interchangers without external cooling [33].

The upper limit of the temperature range for improvement of the Mo_2C/Mo catalyst performance in a hydrogen-rich reaction mixture containing 3 vol.% of CO with a H_2O/CO ratio of 9 and a H_2O/CO_2 ratio of 2, is limited to 700 K by thermodynamic equilibrium. Therefore, the Mo_2C/Mo catalyst can be applied in the temperature range between low- and high temperature WGS catalysts. As described in Section 3.1, the CO reaction order becomes 1 above 590 K. The changes in the H_2O and H_2 partial pressures during the reaction can be neglected. The reaction order in CO_2 becomes 0.1 in the CO_2 partial pressure range of 13–16 kPa (see Eq. (7)). Therefore, for this particular case, Eq. (8) can be simplified to

$$r_{OV} = k'_F \, e^{-E_F/RT} \, p_{CO} - k'_R \, e^{-E_R/RT} \, p_{CO_2}^{0.1} \quad (9)$$

where $k'_F = 3.40 \times 10^{-2}\,Pa^{-1}$ and $k'_R = 5.64 \times 10^{5}\,Pa^{-0.1}$ are the lumped constants of WGS and RWGS reactions, respectively, for a particular reaction mixture composition of 3.0 vol.% CO, 13.5 vol.% CO_2, 27.0 vol.% H_2O, and 56.5 vol.% H_2.

It can be seen that as conversion increases, the maximum of the overall WGS reaction rate shifts to lower temperatures (Fig. 14). When expressed in terms of CO conversion, the optimum temperature (T_{opt}) at a given initial CO partial pressure (p^0_{CO}) and a given CO conversion (x_{CO}) is defined by Eq. (10):

$$\left.\frac{\partial r_{OV}(x_{CO}, p^0_{CO})}{\partial T}\right|_{T=T_{opt}} = 0 \quad (10)$$

Fig. 15 illustrates the optimal temperature profile based on the initial composition of corresponding to the outlet mixture of a HT WGS reactor. At a CO conversion level of 60%, more than a two-fold decrease in the reactor size is possible as a result of temperature gradient in the 530–670 K range.

The results presented in this paper demonstrate that at least an order of magnitude improvement of the performance of the Mo_2C/Mo based catalytic microreactor is still feasible. This can mainly be attained by the improvement in microfabrication and catalytic coating thickness, and by microreactor operation with an optimal temperature profile. The WGS reactor with a Mo_2C/Mo coating can convert up to 75% of carbon monoxide in the temperature range above LT WGS with a traditional Cu/ZnO/Al_2O_3 catalyst. This allows substantial reduction of the size of a LT WGS reactor, which is presently the largest component of a fuel processor.

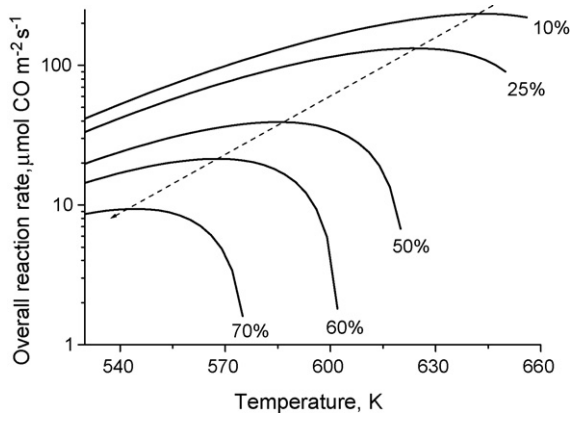

Fig. 14. Overall WGS reaction rate on the Mo_2C/Mo coatings series B estimated by Eq. (8) as a function of temperature and CO conversion. Reaction conditions: p_{CO} = 3.0 kPa, p_{H_2O} = 27.0 kPa, p_{CO_2} = 13.5 kPa, p_{H_2} = 56.5 kPa, balance—He. Total flow: 50 $cm^3\,min^{-1}$ (STP). Dashed line represents the optimal temperature profile in the reactor.

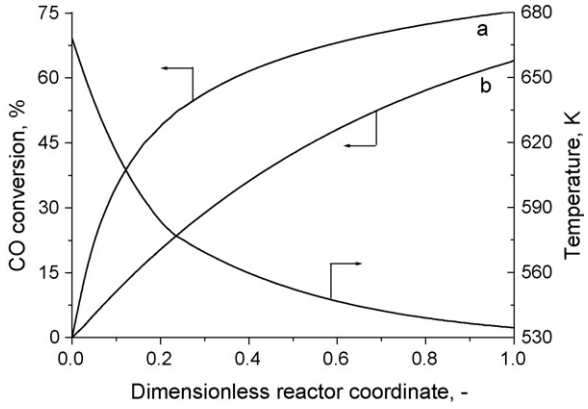

Fig. 15. The optimal temperature profile for the WGS reactor in the 530–670 K temperature range and CO conversion on the Mo_2C/Mo catalyst: (a) with the optimal temperature profile; (b) with an isothermal temperature profile at 530 K. Reaction conditions: p_{CO} = 3.0 kPa, p_{H_2O} = 27.0 kPa, p_{CO_2} = 13.5 kPa, p_{H_2} = 56.5 kPa, balance—He. Total flow: 95 $cm^3\,min^{-1}$ (STP). Mo_2C weight: 80 mg.

4. Conclusions

A new generation of highly active and stable catalytic coatings for application in fuel processors in the water-gas shift reaction has been obtained. The coatings have been synthesized by molten salt synthesis in a melt containing 5 wt.% Li_2CO_3 in an equimolar NaCl–KCl mixture at 1123 K for 7 h. The coatings were stable for more than 500 h on stream at 631 K in a mixture containing 0.5 vol.% CO, 1.5 vol.% H_2O and 40 vol.% H_2. Hexagonal Mo_2C was the only phase present in the coatings. It was shown that if molybdenum carbide is present as a thin layer over a molybdenum substrate (Mo_2C/Mo), the catalytic activity is enhanced compared to that of the pure Mo_2C phase. A combined power-law Eley–Rideal kinetic model is proposed to describe the reaction in the 530–630 K range. This model accurately predicts the equilibrium CO conversion and can be used at H_2O/CO ratios above 1.5, which are typical conditions applied in a fuel processor for fuel cell applications.

Acknowledgements

The financial support by the Netherlands Organisation for Scientific Research (NWO), project no. 047.017.029 and the Russian Foundation for Basic Research (RFBR), project no. 047.011.2005.016, is gratefully acknowledged.

References

[1] J. Patt, D.-J. Moon, C. Phillips, L. Thompson, Catal. Lett. 65 (2000) 193.
[2] D.-J. Moon, J.W. Ryu, Catal. Lett. 92 (2004) 17.
[3] J.S. Lee, S.T. Oyama, M. Boudart, J. Catal. 106 (1987) 125.
[4] P. Seegopaul, L. Gao, Method of using molybdenum carbide catalyst, US Patent 6852303 (2005).
[5] L.T. Thompson, J. Patt, D.-J. Moon, C. Phillips, Transition metal carbides, nitrides and borides, and their oxygen containing analogs useful as water gas shift catalysts, US Patent 6623720 (2003).
[6] H.G. Kim, K.H. Lee, J.S. Lee, Res. Chem. Intermed. 26 (2000) 427.
[7] D.C. LaMont, A.J. Gilligan, A.R.S. Darujati, A.S. Chellappa, W.J. Thomson, Appl. Catal. A 255 (2003) 239.
[8] A.R.S. Darujati, D.C. LaMont, W.J. Thomson, Appl. Catal. A 253 (2003) 397.
[9] Q. Zhu, B. Zhang, J. Zhao, S. Ji, J. Yang, J. Wang, H. Wang, J. Mol. Catal. A 213 (2004) 199.
[10] M. Nagai, K. Matsuda, J. Catal. 238 (2006) 489.
[11] M. Nagai, A.Md. Zahidul, K. Matsuda, Appl. Catal. A 313 (2006) 137.
[12] J.S. Lee, L. Volpe, F.H. Ribeiro, M. Boudart, J. Catal. 112 (1988) 44.
[13] J.S. Lee, M.H. Yeom, K.Y. Park, I.S. Nam, J.S. Chung, Y.G. Kim, S.H. Moon, J. Catal. 128 (1991) 126.
[14] J. Bender, J. Dunn, K. Brezinsky, Microwave-assisted synthesis of carbide and nitride nanolayers on transition metals, in: J. Regalbuto (Ed.), The Science and Engineering of Catalyst Preparation, Marcel Dekker, New York, 2005.
[15] Kh.B. Kushkhov, V.V. Malyshev, L.L. Mazur, V.I. Shapoval, Powder Metall. Met. Ceram. 30 (1991) 392.
[16] V.I. Shapoval, V.V. Malyshev, L.A. Novoselova, Kh.B. Kushkhov, Russ. Chem. Rev. 64 (1995) 125.
[17] S.T. Oyama, Catal. Today 15 (1992) 179.
[18] T. Tsuchida, T. Kakuta, J. Alloys Compd. 398 (2005) 67.
[19] J.G. Chen, Chem. Rev. 96 (1996) 1477.
[20] Y. Gu, Z. Li, L. Chen, Y. Ying, Y. Qian, Mater. Res. Bull. 38 (2003) 1119.
[21] A.Y. Tonkovich, J.L. Zilka, M.J. LaMont, Y. Wang, R.S. Wegeng, Chem. Eng. Sci. 54 (1999) 2947.
[22] E.R. Delsman, M.H.J.M. de Croon, A. Pierik, G.J. Kramer, P.D. Cobden, Ch. Hofmann, V. Cominos, J.C. Schouten, Chem. Eng. Sci. 59 (2004) 4795.
[23] S.A. Kuznetsov, S.V. Kuznetsova, E.V. Rebrov, M.J.M. Mies, M.H.J.M. de Croon, J.C. Schouten, Surf. Coat. Technol. 195 (2005) 182.
[24] N. Floquet, O. Bertrand, J.J. Heizmann, Oxid. Met. 37 (1992) 253.
[25] S.A. Kuznetsov, A.R. Dubrovskiy, E.V. Rebrov, J.C. Schouten, Electrochemical synthesis of Mo_2C catalytical coatings for the water-gas shift reaction, Z. Naturforsch. A, 2007, in press.
[26] D.Yu. Murzin, M.G. Slin'ko, React. Kinet. Catal. Lett. 76 (2002) 369.
[27] C. Wheeler, A. Jhalani, E.J. Klein, S. Tummala, L.D. Schmidt, J. Catal. 223 (2004) 191.
[28] Q. Fu, S. Kudriavtseva, H. Saltsburg, M. Flytzani-Stephanopoulos, Chem. Eng. J. 93 (2003) 41.
[29] R. Keiski, T. Salmi, P. Nienistö, J. Ainassaari, V.J. Pohjola, Appl. Catal. A 137 (1996) 349.
[30] C.V. Ovesen, B.S. Clausen, B.S. Hammershoi, G. Steffensen, T. Askgaard, I. Chorkendorff, J.T. Norskov, P.B. Rasmussen, P. Stoltze, P. Taylor, J. Catal. 158 (1996) 170.
[31] G. Kolb, H. Pennemann, R. Zapf, Catal. Today 110 (2005) 121.
[32] G.-Y. Kim, J.R. Mayor, J. Ni, Chem. Eng. J. 110 (2005) 1.
[33] W. Nicol, D. Hildebrandt, D. Glasser, Comput. Chem. Eng. 26 (2002) 803.